PERGAMON

Carbon 40 (2002) 929–937

CARBON

# Microstructure of carbon blacks determined by X-ray diffraction profile analysis

Tamás Ungár[a,*], Jenő Gubicza[a], Gábor Ribárik[a], Cristian Pantea[b], T. Waldek Zerda[b]

[a]*Eötvös University, Department of General Physics, P.O. Box 32, Budapest, H-1518 Hungary*
[b]*TCU, Department of Physics, Fort Worth, TX 76129, USA*

Received 18 April 2001; accepted 21 August 2001

**Abstract**

The microstructure of carbon blacks is investigated by X-ray diffraction peak profile analysis. Strain anisotropy is accounted for by the dislocation model of the mean square strain in terms of average dislocation contrast factors. Crystallite shape anisotropy is modeled by ellipsoids incorporated into the size profile function. Different grades of carbon blacks, N990, N774 and N134, untreated, heat-treated and compressed at 2.5 GPa have been investigated. The microstructure is characterized in terms of crystallite size-distribution, dislocation density and crystallite shape anisotropy. Heat treatment results in increased vertical and lateral sizes of graphitic crystallites. Postproduction pressure treatment has little effect on the average sizes of the crystallites, however, it affects the crystallite size distribution function. The average sizes of the crystallites obtained by X-ray diffraction agree with those estimated from Raman spectra. Applied pressure affects the magnitude of strain within the crystallites. 

*Keywords:* A. Carbon black; B. High pressure; C. X-ray diffraction; D. Crystallite size

## 1. Introduction

Carbon black is generally used as a filler in rubber production to modify the mechanical properties of the tire. Although the smallest indivisible unit of carbon black is the aggregate, in the TEM images aggregates appear to be formed by spherical particles, which are fused together. Aggregates connect through Van der Waals forces into networks called agglomerates [1]. The internal structure of aggregates is not well understood. Graphite-like, quasicrystalline domains, in which basal planes are parallel but angularly distorted and the spacing between the layers is different from that of pure graphite, have been detected in carbon black particles [1]. Biscoe and Warren identified those structures as intermediate between crystalline and amorphous materials [2]. Hereafter, the turbostratic quasi-crystalline domains are referred to as graphitic crystallites or nanocrystallites. Due to the lack of three-dimensional ordering, this nomenclature is not rigorously correct, but appears to be generally accepted in the scientific literature [1–5]. The layer stacking disorder can be observed in principle by analysing HK bands in the diffractograms. Rocking curves of the HK.0 type reflections would show extra broadening due to rotations around the hexagonal *c* axis whereas the 00.L type reflections would be broader in the $\theta$–$2\theta$ radial direction. This kind of layer stacking disorder can be handled as effective boundaries of coherently scattering domains where diffraction peak broadening is a measure of the size of these objects.

The structure of carbon black particles and their surface properties are important for many reasons. Different sites present on the surface determine reinforcing properties of carbon black in rubber [6]. Energy of interaction between the polymer and carbon black depends on nature and population of different sites. The most energetic sites, which very effectively adsorb polymers, are usually identified as crystallite edges. Crystallite flat surfaces and amorphous carbon present on the surface are considered less energetic sites. Thus to characterize reinforcing properties of carbon black it is necessary to determine the fraction of the surface occupied by amorphous carbon and estimate the size of the crystallites and their surface density. Relative concentration of amorphous carbon can

*Corresponding author. Fax: +36-1-372-2811.
*E-mail address:* ungar@ludens.elte.hu (T. Ungár).

0008-6223/02/$ – see front matter 
PII: S0008-6223(01)00224-X

be evaluated from Raman measurements [3]. Energies of adsorption of different adsorption sites and their relative populations have recently been evaluated by gas adsorption technique [7]. The sizes of graphitic crystallites have been estimated from X-ray diffraction [5,8], neutron scattering [9], atomic force microscopy [10], and Raman spectroscopy measurements [3–5]. Those studies showed that the average size of crystallites, $L_a$, is similar for all commercial carbon black grades produced in furnace reactors and roughly equal 2.3 nm. This was a surprising result because different grades have completely different rubber reinforcing properties.

Small crystallites are not energetically favorable structures. One possible explanation for their presence in carbon blacks is that large strains are developed in production, i.e. during aggregate growth at high temperatures and also during water quenching, when the temperature of carbon black is rapidly reduced from about 1600°C to about 800°C. Strain is relieved when larger structures break to form smaller crystallites. Characterization of strain remaining in the crystallites is an important problem, which so far has not been addressed. Strain can change bond lengths and angles, and thus affect surface potential and in turn reinforcing properties of carbon blacks. Reinforcing properties of carbon black are also expected to be a function of crystallite size distribution. Carbon black with uniform crystallites that all have similar sizes is expected to have more homogenous surface potential than carbon black exhibiting a wide distribution of sizes.

X-ray diffraction peak profile analysis is a widely used method for the determination of crystallite size and lattice defect structure in crystalline materials. The evaluation procedures are based on the different diffraction order dependence of size and strain broadening. In the simplest case the size broadening is independent while the strain broadening is dependent on the diffraction order. Both dependencies become, however, complicated if shape or strain are anisotropic. Shape anisotropy has been modeled by cylindrical [11] bodies and strain anisotropy has been accounted for either by a phenomenological model of anisotropic elastic constants [12] or by the anisotropic strain fields of dislocations [13,14]. The size-distribution of spherical crystallites has been recently suggested to be determined by whole profile fitting in the absence of strain by using theoretically calculated size profiles [15].

In the present work it is shown that theoretical diffraction profiles can be constructed in the presence of lattice distortions using the strain profile derived by Wilkens for dislocated crystals [16]. A procedure is described in which the Fourier coefficients of the experimentally determined physical peak profiles are fitted by the Fourier transforms of ab initio size and strain profiles. In this method the strain is assumed to be caused by dislocations and the crystallites are modeled by ellipsoids with log-normal size distribution. The only fitting parameters are well established physical parameters being characteristic of the microstructure: (i) $m$ and (ii) $\sigma$, the median and the variance of the log-normal crystallite size distribution function, (iii) the ellipticity of crystallite shape, (iv) $\rho$ and (v) $M$, the density and the arrangement parameter of dislocations and (vi) $q$ or $A$ and $B$, the relevant parameters describing the average dislocation contrast factors in cubic or hexagonal crystals, respectively.

In this paper the effect of annealing and pressure on (a) the size distribution and (b) the shape of crystallites as well as (c) the strain (dislocation density) in the crystallites of different grades of carbon black samples is studied by X-ray diffraction profile analysis. The values of the average crystallite sizes determined by X-rays were compared with those obtained from Raman measurements.

## 2. Evaluation of X-ray diffraction profiles

### *2.1. The method of whole profile fitting by Fourier coefficients (WPFC)*

Within the kinematical theory of X-ray diffraction the physical profile of a Bragg reflection is given by the convolution of the size and the distortion profiles [17]:

$$I^{\mathrm{P}} = I^{\mathrm{S}} \times I^{\mathrm{D}}, \tag{1}$$

where the superscripts S and D stand for size and distortion, respectively. It follows from Eq. (1) that the Fourier coefficients of the physical profile are the production of the Fourier coefficients of the size and strain profiles:

$$A(L) = A^{\mathrm{S}}(L)\, A^{\mathrm{D}}(L), \tag{2}$$

where $A(L)$ are the absolute values of the Fourier coefficients of the physical profiles, $A^{\mathrm{S}}$ and $A^{\mathrm{D}}$ are the size and the distortion Fourier coefficients and $L$ is the Fourier variable.

In the case of spherical crystallites, size broadening is diffraction order independent [18]. Raman spectroscopy has shown that the carbon black crystallites are non-spherical flat discs [3–5]. Since the size broadening caused by non-spherical crystallites is diffraction order dependent, the size profiles of ellipsoids of revolution have been elaborated. A brief description of this derivation is given below. It is assumed that ellipticity, $\varepsilon$, the ratio of the diameters $D_c$ and $D_a$, parallel and perpendicular to the axis of revolution, is the same for all crystallites, and that the crystallite size distribution density function, f($x$), is log-normal:

$$\mathrm{f}(x) = \frac{1}{\sqrt{2\pi}\sigma}\frac{1}{x}\exp\left\{-\frac{[\ln(x/m)]^2}{2\sigma^2}\right\}, \tag{3}$$

where $\sigma$ is the variance and $m$ is the median of the size distribution density function f($x$). According to Bertaut [19] and Guinier [20] the size part of the Fourier transform

of the (*hkl*) diffraction peak at a given value of the Fourier variable $L$ can be calculated as the common volume to the crystal and its 'ghost' obtained by a translation by $L$ in the direction normal to the reflecting *hkl* planes. To calculate the Fourier transform corresponding to a crystallite, divide the crystal into cylindrical columns normal to the *hkl* lattice planes and set $\mathrm{d}\sigma_\mu$ for the cross section of the column with the height $\mu$ [20]. The volume common to this column and its ghost is:

$$A^{\mathrm{S}}(L) = \left(1 - \frac{|L|}{\mu}\right)\mu \, \mathrm{d}\sigma_\mu. \tag{4}$$

The common volume to the irradiated crystallites and to their 'ghosts' shifted by $L$ can be obtained by summing for all columns existing in the crystallites. Let us set $\alpha$ as the angle between the axis of revolution and the diffraction vector with the indices *hkl*. Summing up the common volumes of the columns parallel to the diffraction vector for one crystallite the following formula is obtained for the normalized size Fourier transform:

$$A^{\mathrm{S}}(L) = \begin{cases} 1 - \dfrac{3|L|}{2D_{hkl}} + \dfrac{|L|^3}{2D_{hkl}^3} & \text{if} \quad |L| \le D_{hkl} \\ 0 & \text{if} \quad |L| \ge D_{hkl} \end{cases} \tag{5}$$

where $D_{hkl}$ is the diameter of the ellipsoid in the *hkl* direction which can be given in terms of $\alpha$:

$$D_{hkl} = \frac{D_{\mathrm{a}}}{\sqrt{\sin^2\alpha + \dfrac{\cos^2\alpha}{\varepsilon^2}}} \tag{6}$$

where $D_{\mathrm{a}}$ is the diameter of the ellipsoid perpendicular to the axis of revolution. Making the summation for all the crystallites having the log-normal size distribution the following formula is obtained for the normalised size Fourier transform:

$$\begin{aligned} A^{\mathrm{S}}(L) = {} & \frac{1}{2}\,\mathrm{erfc}\left[\frac{\ln(|L|/m_{hkl})}{\sqrt{2}\sigma} - 1.5\sqrt{2}\sigma\right] \\ & - \frac{3}{4m_{hkl}\exp(8.125\sigma^2)}\,|L|\,\mathrm{erfc}\left[\frac{\ln(|L|/m_{hkl})}{\sqrt{2}\sigma} - \sqrt{2}\sigma\right] \\ & + \frac{3}{4m_{hkl}^3\exp(10.125\sigma^2)}\,|L|^3\,\mathrm{erfc}\left[\frac{\ln(|L|/m_{hkl})}{\sqrt{2}\sigma}\right] \end{aligned} \tag{7}$$

where erfc is the complementary error function defined as:

$$\mathrm{erfc}(x) = \frac{2}{\sqrt{\pi}}\int_x^\infty \exp(-t^2)\mathrm{d}t, \tag{8}$$

and $m_{hkl}$ is the median of the distribution of diameters in the *hkl* direction given as:

$$m_{hkl} = \frac{m_{\mathrm{a}}}{\sqrt{1 + \left(\dfrac{1}{\varepsilon^2} - 1\right)\cos^2\alpha}} \tag{9}$$

where $m_{\mathrm{a}}$ is the median of the size distribution of diameters of ellipsoids perpendicular to the axis of revolution. If the relative orientations of the crystallographic directions to the axis of revolution are known, $\cos\alpha$ can be expressed by the indices of reflection. The axis of revolution is taken to be perpendicular to the basal plane of hexagonal carbon black crystals, therefore $\cos\alpha$ can be given as:

$$\cos\alpha = \frac{l}{\sqrt{\dfrac{4}{3}\dfrac{c^2}{a^2}(h^2 + k^2 + hk) + l^2}}, \tag{10}$$

where $c/a$ is the ratio of the lattice constants of the hexagonal crystal.

The diffraction profiles can be broadened due to the strain field of the lattice defects in the crystal. The point defects have diffraction effects far from the fundamental Bragg reflections, often called Huang scattering, because of their short-range strain field [21]. The strain fields of dislocations are of long-range character, therefore their diffraction effects cluster around the fundamental Bragg reflections. This diffraction effect is called the diffraction peak broadening. The strain fields of planar defects are space independent thus, in the first approximation, they cause lattice parameter changes and shift Bragg reflections. In reality lattice defects are more complex and their effects on peak shape can be a mixture of three well-separated cases: (i) Huang scattering, (ii) peak broadening and (iii) peak shifts. Stacking faults, for example, can cause peak shifts and peak broadening simultaneously since they are usually bounded by partial dislocations. Despite this complex behaviour, dislocations play a special and unique role: they are always present (1) either as the major component in complex lattice defects or (2) as the only lattice defects which distort the crystal lattice to such an extent that it becomes visible as profile (or line) broadening in a diffraction experiment. For this reason, in the present account we consider the effect of dislocations on strain broadening.

Assuming that in the crystal the lattice distortions are caused by dislocations, the Fourier coefficients of the strain profile can be given as [16,22]

$$A_g^{\mathrm{D}}(L) = \exp[-\rho B L^2\,\mathrm{f}(\eta)\,g^2\bar{C}], \tag{11}$$

where $g$ is the length of the diffraction vector, $B = \pi b^2/2$, where $b$ is the length of the Burgers vector, $\eta \sim L/R_{\mathrm{e}}$, where $R_{\mathrm{e}}$ is the outer cut off radius of dislocations, $\rho$ and $C$ are the density and the contrast factors of dislocations and $\mathrm{f}(\eta)$ is the $L$ dependence part of the mean square strain in a dislocated crystal. In the following $\mathrm{f}(\eta)$ will be called the Wilkens function. This function starts with a logarithmic term and continues as a hyperbola for large $L$ values:

$$\mathrm{f}(\eta) \sim -\ln\eta + \left(\frac{7}{4} - \ln 2\right) + \cdots \text{ for } \eta \le 1 \tag{12}$$

$$f(\eta) \sim -\frac{512}{90\pi}\frac{1}{\eta} + \cdots \text{ for } \eta \geq 1. \quad (13)$$

The detailed expressions for $f(\eta)$ are given in Eqs. A.6 to A.8 in Ref. [16] and have been cited in Eqs. (22) and (23) in Ref. [18]. In the procedure developed here the full expressions in A.6 to A.8 in Ref. [16] were used. It is physically more appropriate to use the dimensionless parameter $M = R_e\sqrt{\rho}$ defined by Wilkens as the dislocation arrangement parameter [23]. The value of $M$ gives the strength of the dipole character of dislocations: the higher the value of $M$, the weaker the dipole character and the screening of the displacement field of dislocations.

The average dislocation contrast factors are the weighted average of the individual $C$ factors either over the dislocation population or over the permutations of the *hkl* indices [22–24]. Based on the theory of line broadening caused by dislocations it can be shown that in an untextured hexagonal polycrystalline specimen the values of $\overline{C}$ are simple functions of the invariants of the fourth order polynomials of *hkl* [25]:

$$\overline{C} = \overline{C}_{hk0}\left[1 + \frac{[A(h^2+k^2+(h+k)^2) + Bl^2]l^2}{\left[h^2+k^2+(h+k)^2 + \frac{3}{2}\left(\frac{a}{c}\right)^2 l^2\right]^2}\right] \quad (14)$$

where $\overline{C}_{hk0}$ is the average dislocation contrast factor for the *hk*0 reflections, $A$ and $B$ are parameters depending on the elastic constants and on the character of dislocations (e.g. edge or screw type) in the crystal and $c/a$ is the ratio of the two lattice constants of the hexagonal crystal.

A numerical procedure has been worked out for fitting the Fourier transform of the experimental profiles by the product of the theoretical functions of size and strain Fourier transforms given in Eqs. (7)–(10) and (11)–(14), respectively [26,27]. The method has the following steps: (i) the Fourier coefficients of the measured physical profiles have been calculated by a non-equidistant sampling Fourier transformation, (ii) the Fourier coefficients of the size and strain profiles were calculated using Eqs. (7)–(10) and (11)–(14), respectively, (iii) the experimental and the calculated Fourier coefficients were compared by the least squares method. The procedure has seven fitting parameters for the hexagonal carbon black materials: (i) the median, $m$, and (ii) the variance, $\sigma$, of the log-normal crystallite size distribution function, (iii) the ellipticity of the crystallite shape, $\varepsilon$, (iv) the density, $\rho$, and (v) the arrangement parameter, $M$, of dislocations and (vi–vii) the parameters $A$ and $B$ for the average dislocation contrast factors. Further details of the fitting procedure are given elsewhere [26,27].

### *2.2. Corrections for instrumental effects, background and overlapping peaks*

For the carbon black powder samples strong overlap of the diffraction profiles has been observed. The overlapping peaks have to be separated since the present evaluation method is worked out for individual profiles. Background subtraction and the separation of overlapping peaks are carried out in one step. Two or more analytical functions, usually of PearsonVII or Pseudo-Voigt type plus a linear or second order polynomial background are fitted to the overlapping peaks. Background correction was carried out after the diffractograms have been rescaled to 2 sin $\theta/\lambda$ instead of $2\theta$. This procedure enables the correct background subtraction even in the presence of non-negligible small angle scattering contributions. In the next step the unwanted fitted peaks together with the linear background are subtracted leaving the targeted peak free of overlap and background. The procedure is then repeated for other targeted peaks. The separated profiles are taken as individual diffraction profiles in the evaluation procedures. Due to very large strains and nanometer size crystallites, peak broadening of the carbon black specimens is about two orders of magnitude larger than the instrumental effects. For this reason no instrumental corrections were carried out.

## 3. Experimental

### *3.1. Sample preparation*

Three different grades of carbon blacks were selected for this study, N990, N774 and N134. They differ in average aggregate diameters ranging from 285 nm (N990) to 18 nm (N134), surface area ranging from 8.5 $m^2/g$ (N990) to 145 $m^2/g$ (N134), and their reinforcing properties (N134 is mainly used in tread applications while N774 is used in tire carcasses, for example). N134 and N774 are obtained in furnace reactors using similar processes. N990 is a thermal black and is produced by thermal decomposition of hydrocarbon gases in the absence of a flame.

Carbon blacks were heat-treated for 20 min at 2700°C and those samples are labeled as G (graphitized). To avoid oxidation the chamber of the induction furnace was purged and filled with gaseous nitrogen. After the heat-treatment the samples were allowed to cool down slowly to room temperature. High pressure experiments were conducted at room temperature inside a piston cylinder cell at the pressure of 2.5 GPa (25,000 bar). The samples were allowed to remain compressed for about 20 min. The raw carbon blacks exposed to high pressure are denoted as P, those which first underwent heat treatment are called PG. The specimen N134 was not subjected to high pressure experiments therefore P134 is absent from the series.

### *3.2. X-ray diffraction technique*

Two different X-ray diffractometers were used for the

analysis of peak profiles. (i) A conventional $\theta$–$2\theta$ diffractometer was used to obtain an overview of the diffractograms, (ii) the individual peak profiles were measured in a special double crystal high resolution diffractometer with negligible instrumental broadening. The first (i) diffractometer was a Philips X'pert diffractometer using Cu anode and pyrolitic graphite secondary monochromator. The second (ii) diffractometer (Nonius FR 591) enables a better separation of the overlapping peaks due to the absence of the K alpha doublet. In this diffractometer a fine focus rotating cobalt anode was operated as a line focus at 36 kV and 50 mA ($\lambda = 0.1789$ nm). The symmetrical 220 reflection of a Ge monochromator was used in order to have wavelength compensation at the position of the detector. The $K_{\alpha_2}$ component of the Co radiation was eliminated by a 0.16 mm slit between the source and the Ge crystal. The profiles were registered by a linear position sensitive gas flow detector, OED 50 Braun, Munich. In order to avoid air scattering and absorption the distance between the specimen and the detector was overbridged by an evacuated tube closed by mylar windows. Seven diffraction peaks indexed as 0002, 10$\underline{1}$0, 10$\underline{1}$1, 0004, 11$\underline{2}$0, 11$\underline{2}$2 and 0006 were recorded. 10$\underline{1}$0 and 10$\underline{1}$1 as well as 11$\underline{2}$0, 11$\underline{2}$2 and 0006 overlap and were separated by fitting procedures. The most intense five profiles 0002, 10$\underline{1}$0, 10$\underline{1}$1, 0004 and 11$\underline{2}$0 were used in the evaluation method.

### 3.3. Raman spectroscopy

Complementary data on average sizes of graphitic crystallites were obtained from Raman scattering measurements. In addition, Raman studies allowed us to estimate the relative concentration of amorphous carbon on the surface of carbon black aggregates. Raman spectra were obtained using a home-made spectrometer equipped with a confocal microscope. To avoid laser heating carbon blacks were placed inside a groove in a steel disk spinning at a speed of 3000 rev./min. The average size of nanocrystallites can be determined in terms of changes in position, width and intensity ratio of two Raman peaks observed at 1345 $cm^{-1}$ (the disordered, or d peak) and 1575 $cm^{-1}$ (the graphite, or g peak). The shape of those peaks depends on the crystallite sizes. When the crystallites become larger, the peaks become narrower, their maxima move to higher frequencies and the intensity of the g peak systematically increases in comparison with the d peak. Using the empirical formula found by Tuinstra and Koenig [28]

$$L_a = 4.35\, I_g / I_d \,(\text{nm}) \tag{16}$$

it is possible to evaluate $L_a$, the lateral size of the crystallites. Amorphous carbon is observed as a broad peak centered at about 1530 $cm^{-1}$. Its intensity relative to that of the d and g peaks is an estimate of the relative concentration of amorphous carbon on the surface of carbon black aggregates [3].

## 4. Results and discussion

### 4.1. Average size, size distribution and shape of crystallites

The typical powder patterns for the initial N774 and the graphitized G774 samples are shown in Fig. 1a and b, respectively. It can be seen that after heat treatment at 2700°C the peak profiles become rather narrow. Note that in Fig. 1b the intensity is scaled logarithmically in order to show the details of the peaks at lower intensities. The diffractograms show strong overlap of the peaks for both samples. The overlapping peaks were measured by the double crystal diffractometer and were separated by the method described in Section 2.2. The Fourier coefficients of the measured profiles for N774 sample and the fitted ab initio functions normalized to unity are shown in Fig. 2. There is a good agreement between the two sets of data. The measured and separated profiles and the inverse Fourier transform of the fitted Fourier coefficients normalized to unity for N774 are shown in Fig. 3. Again a good

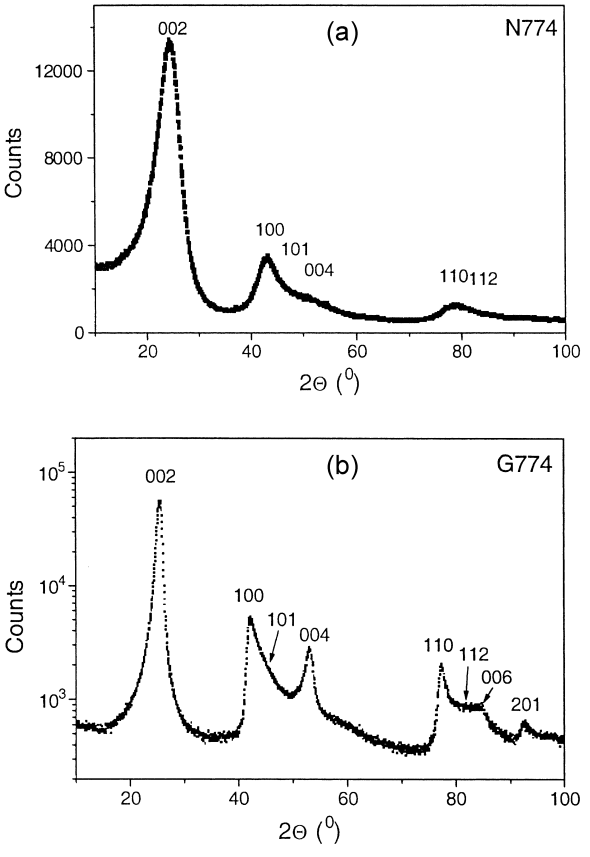


Fig. 1. The powder diffractograms for the N774 carbon black specimen in the initial state (a) and for the specimen G774 after annealing at 2700°C (b). The intensity in logarithmic scale in (b) shows details of low intensity peaks.

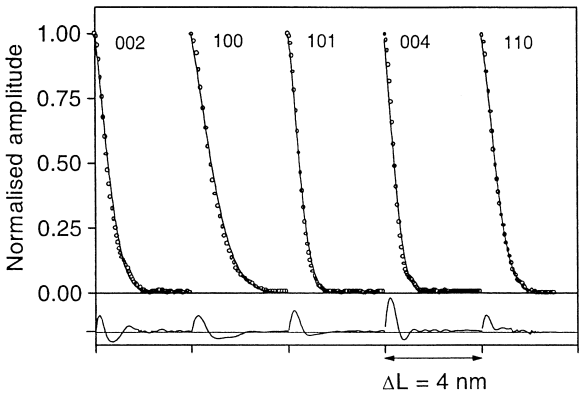


Fig. 2. The Fourier coefficients of the measured (open circles) and the fitted theoretical functions (solid lines), normalized to unity for the specimen N774. The differences between fitted and measured data and the indices of reflections are indicated.

correlation between the measured and the fitted data can be observed. The median, $m_a$, and the variance, $\sigma$, of the size distribution of the crystallite diameter parallel to the hexagonal basal plane, the ellipticity of the crystallite shape, $\varepsilon$, and the density, $\rho$, of dislocations are determined from the fitting procedure and listed in Table 1.

Raman spectra of carbon blacks were resolved into two components by a fitting procedure as shown in Fig. 4 for the sample N134. The ratio of these two components gives the average lateral sizes of the crystallites parallel to the hexagonal basal plane. The precision of the fitting routine was better than 10% and reproducibility was better than 5%. The calculated $L_a$ values are listed in Table 1. Comparing these values to the median diameter data, $m_a$, obtained from X-ray analysis it is seen that both techniques give similar results. As expected, $m_a$ values increase with increasing diameters of the aggregates in the order — N134, N774, and N990. The agreement between the data from X-ray diffraction and Raman measurements is usually better than 25%. The discrepancies for the samples N990 can be explained as follows. X-rays easily penetrate through carbon blacks and the line profiles are determined by scattering on graphitic layers present throughout the material. On the other hand, Raman intensity is strongly attenuated by carboneous materials and 30% of the Raman intensity originates from layers lying less than 10 nm below the surface, and 90% from the outer layer of thickness less than 40 nm [29]. It is possible that for the samples N990 with average aggregate diameter of about 285 nm, large crystallites are present under the skin layer and thus are not detected by Raman. For other grades of small aggregate diameters it is safe to assume that the Raman signal originates from groups distributed throughout the sample.

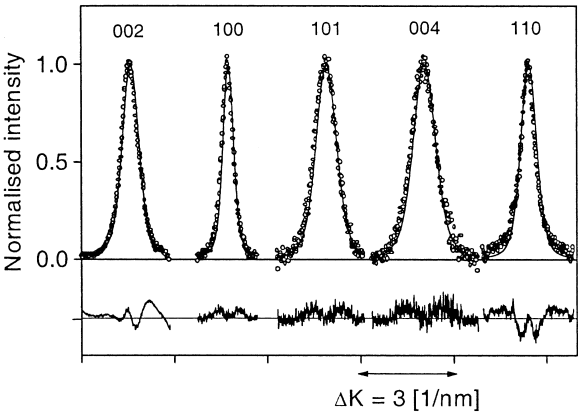


Fig. 3. The measured intensity profiles (open circles) and the inverse Fourier transforms of the fitted Fourier coefficients (solid lines), normalized to unity. The differences between fitted and measured data and the indices of reflections are indicated.

Crystallites were approximated by ellipsoids and $m_c$ is the median of the diameters of the crystallites perpendicular to the hexagonal basal plane, i.e. it measures the stacking heights of graphitic nanocrystallites. In good agreement with previous studies the value of $\varepsilon = m_c/m_a$ is between 0.5 and 1.0, i.e. the heights of the crystallites vary between 50 and 100% of their corresponding lateral sizes.

The shape and the size of crystallites vary significantly in different grades of carbon black as well within the same specimen due to pressure and heat-treatment. The calculated size distributions for different grades are compared in Fig. 5. For N990 the average size of the crystallites is only 5.6 nm, but Fig. 5 indicates that for this carbon it is possible to find crystallites as large as 16 nm across. Different shapes for the size distribution function obtained for different grades are probably associated with different production conditions, such as temperature, speed of the reaction, composition of the feedstock, the residence time in the flame zone, and the position of quenching zone.

Heat treatment increases the average sizes of graphitic crystallites. This effect has been observed before by Raman, TEM, AFM, and also by X-ray diffraction using the Scherrer method. These techniques proved that at elevated temperatures crystallites grow both in the lateral and vertical directions. This study confirmed this result. In the untreated samples the lateral sizes of crystallites ($L_a$ or $m_a$) are usually twice the size of the stacking height of the layers, $m_c$. But after heat treatment the lateral and vertical dimensions become similar, compare Table 1. These effects are accompanied by modifications of the shapes of the distribution functions, which for graphitized carbons become more asymmetric. Concentration of amorphous carbon is reduced after heat treatment. Practically no significant contribution can be detected in samples heated to 2700°C.

Hydrostatic pressure did not change the average sizes of graphitic crystallites (both in the initial and the graphitized states), with the exception of the P990 where the crystallites became significantly smaller. The crystallite size

Table 1
Lateral crystallite size, $L_a$, and relative content of amorphous carbon, $I_a/I_{total}$, obtained from Raman spectroscopy; the median, $m_a$, and the variance, $\sigma$, of the distribution of the crystallite-diameters parallel to the hexagonal basal plane, the ellipticity of the crystallite shape and the dislocation density, $\rho$, (strain) determined by X-ray diffraction for carbon blacks of different grades and various histories of temperature and pressure treatments

| Sample | $\varepsilon = D_c/D_a$ | $L_a$ (nm) Raman | $m_a$ (nm) | $\sigma$ | $\rho$ ($10^{15}$ m$^{-2}$) | $I_a/I_{total}$ Raman |
|---|---|---|---|---|---|---|
| N134 | 0.5 | 1.8 | 1.9 | 0.37 | 560 | 0.16 |
| G134 | 0.9 | 6.6 | 6.4 | 0.2 | 11 | 0.00 |
| PG134 | 0.8 | 6.7 | 8.3 | 0.09 | 53 | 0.02 |
| N774 | 0.5 | 2.3 | 2.7 | 0.31 | 130 | 0.24 |
| P774 | 0.6 | 2.8 | 3.6 | 0.16 | 300 | 0.20 |
| G774 | 1.2 | 11.5 | 11.3 | 0.02 | 14 | 0.02 |
| PG774 | 1.0 | 11.6 | 11.4 | 0.025 | 153 | 0.01 |
| N990 | 0.6 | 3.6 | 5.6 | 0.45 | 54 | 0.10 |
| P990 | 0.5 | 3.8 | 2.6 | 0.45 | 137 | 0.09 |
| G990 | 1.1 | 18.1 | 11.0 | 0.49 | 5.5 | 0.01 |
| PG990 | 1.0 | 13.0 | 6.1 | 0.18 | 26 | 0.00 |

distributions for the specimen N990 in the initial state as well after heat-treatment and pressure-treatment are shown in Fig. 6. In the case of this particular carbon black, before heat-treatment the largest crystallites approach 16 nm. External pressure might break those large crystallites into smaller units and as a result the distribution function becomes less asymmetric and its maximum is shifted toward lower $L_a$ values. This effect is also clearly seen for other carbon blacks. The distribution functions become narrower and more symmetric indicating that in those samples larger crystallites are reduced to smaller ones. Our previous neutron scattering and Raman in situ high-pressure studies on carbon blacks indicated that under pressure the turbostratic structures become organized and carbon–carbon bonds approach values typical for a graphite crystal [4]. The current study was conducted after the pressure treatment and since we did not observe any significant changes in the crystallite sizes we concluded that the system returned to its original configuration.

Pressure was also applied to previously graphitized carbon blacks. No significant changes in the sizes have been observed. However, the distribution functions all

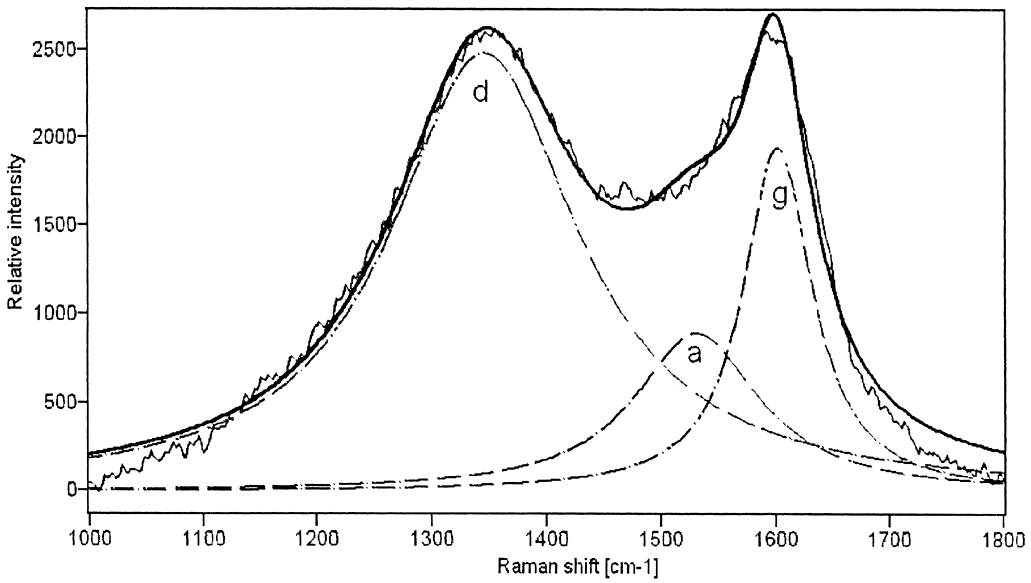


Fig. 4. Raman spectrum of the specimen N134. Solid line, the best fit to a sum of three components. Disordered, d, amorphous, a, and graphitic, g, components are shown as broken lines.

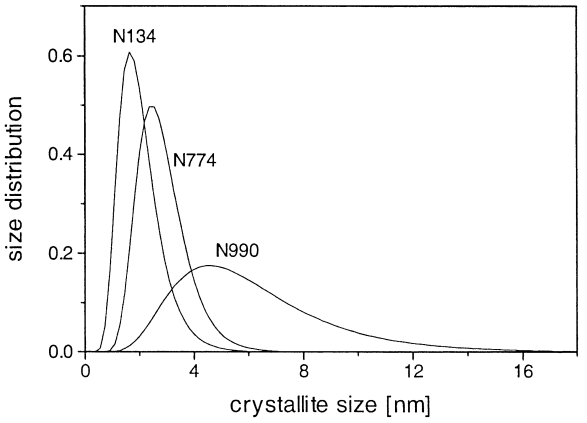


Fig. 5. Crystallite size distribution for N134; N774 and N990.

became very narrow. It indicates that larger crystallites are reduced to smaller units but in a way that leaves the average value unchanged. After pressure treatment concentration of amorphous carbon either slightly decreased or remained unchanged.

### *4.2. Dislocation density (strain)*

The magnitude of strain is characterized by the dislocation density, $\rho$. In the untreated samples its values are very large, of the order of $10^{16}$ $m^{-2}$ (see Table 1). Population of dislocations or the magnitude of strain dramatically decreases with graphitization but increases after pressure treatment. This is an expected result. High temperature treatment followed by slow cooling anneals the samples and decreases the magnitude of strain. Hydrostatic pressure used in this study did not break crystallites into smaller units but was sufficient to induce strain. Pressure treatment of previously graphitized samples also resulted in increased values of $\rho$.

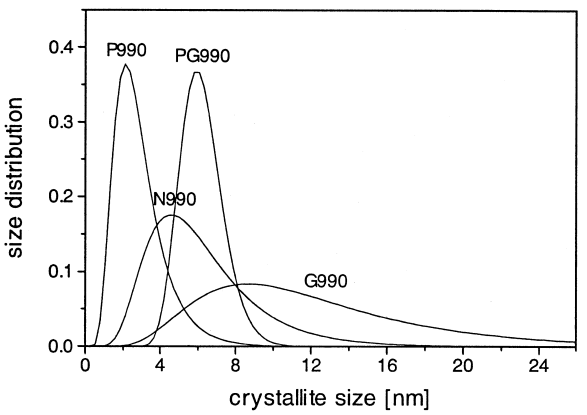


Fig. 6. Crystallite size distribution for the as-received specimen N990, after heat treatment at 2700°C, after pressure treatment at 2.5 GPa, and graphitized black after pressure treatment.

## 5. Conclusions

A procedure has been developed to evaluate X-ray diffraction peak profiles using the Fourier coefficients of ab initio theoretical size and strain profiles. The crystallites are modeled by ellipsoids with log-normal size distribution and the strain is assumed to be caused by dislocations. The procedure enables the determination of the median and the variance of the crystallite size distribution, the ellipticity of the crystallite shape and the dislocation density. This method was applied to different grades of carbon black powders before and after heat- and pressure-treatments.

The average crystallite size is found to be in the nanometer scale for all carbon black powders. Different average sizes and size distributions of crystallites have been identified in different grades of furnace carbon blacks, which is explained by the difference in the production conditions. It was found that for carbon blacks of large aggregates, the chance of finding large crystallites is increased. The average crystallite sizes determined by X-rays agree well with Raman results except for the samples N990. For these specimens Raman measurements indicate smaller crystallites than those measured by X-rays because the Raman spectra are mainly due to the outer skin of the aggregates while X-ray diffraction detects crystallites throughout the volume. In the untreated samples the lateral sizes of crystallites are usually twice the size of the stacking height of the layers.

Heat-treatment increases the average sizes of graphitic crystallites and the lateral and vertical dimensions of the crystallites become similar. The dislocation density is increased during annealing. Concentration of amorphous carbon is decreased upon heat treatment. We interpret this observation as a result of amorphous carbon being gradually incorporated into graphitic layers.

The pressure-treatment has no significant effect on the size and the shape of the crystallites and the population of amorphous carbon while the dislocation density (or strain) in the crystallites has been increased.

## Acknowledgements

The authors are grateful for the financial support of the Hungarian Scientific Research Fund, OTKA, grant nos. T031786, T034666 and D-29339 and Texas Advanced Technology Program. We thank Dr. M. Gerspacher, Sid Richardson Carbon Co., for numerous discussions.

## References


[1] Donnet JB, Voet A. In: Carbon black. Physics, chemistry and elastomer reinforcement, New York: Dekker, 1976, pp. 50–118.
[2] Biscoe J, Warren BE. J Appl Phys 1942;13:364–72.
[3] Zerda TW, Xu W, Yuang H, Gerspacher M. Rubber Chem Technol 1998;71:26–37.
[4] Zerda TW, Xu W, Zerda A, Zhao Y, Von Dreele RB. Carbon 2000;38:355–64.
[5] Gruber T, Zerda TW, Gerspacher M. Carbon 1994;2:1377–82.
[6] Gerspacher M, O'Farrell CP, Wampler WA. Rubber World 1995;212:26–9.
[7] Schuster R, Schroeder A. Proceedings of ACS Rubber Division Meeting, Dallas, April 2000, submitted to Kautschuk, Gummi, Kunststoffe.
[8] Zerda TW, Pantea C, Qian J, Ungár T. In: Hjelm RP, Nakatani AI, Gerspacher M, Krishnamoorti R, editors, Proceedings MRS Fall meeting, symposium: filled and nanocomposite polymer materials, Boston, USA, 2000, KK6.4.1-8.
[9] Hjelm R, Wampler WA, Seeger PA, Gerspacher M. J Mater Res 1994;9:3210–22.
[10] Xu W, Zerda TW, Raab H, Goritz D. Carbon 1997;35:471–4.
[11] Louër D, Auffredic JP, Langford JI, Ciosmak D, Niepce JC. J Appl Cryst 1983;16:183–91.
[12] Stephens PW. J Appl Cryst 1999;32:281–8.
[13] Ungár T, Borbély A. Appl Phys Lett 1996;69:3173–5.
[14] Ungár T, Dragomir I, Révész Á, Borbély A. J Appl Cryst 1999;32:992–1002.
[15] Langford JI, Louer D, Scardi P. J Appl Cryst 2000;33:964–74.
[16] Wilkens M. In: Simmons JA, de Wit R, Bullough R, editors, Fundamental aspects of dislocation theory, vol. II, Washington, DC: National Bureau of Standards (US), 1970, pp. 1195–221, Special publication no. 317.
[17] Warren BE, Averbach BLJ. Appl Phys 1950;21:595–610.
[18] Ungár T, Gubicza J, Ribárik G, Borbély A. J Appl Cryst 2001;34:298–310.
[19] Bertaut EF. Acta Cryst 1950;3:14–9.
[20] Guinier A. X-ray diffraction. San Francisco, CA: Freeman, 1963.
[21] Trinkaus H. Phys Stat Sol (b) 1972;51:307–19.
[22] Krivoglaz MA. Theory of X-ray and thermal neutron scattering by real crystals. New York: Plenum Press, 1969.
[23] Wilkens M. Phys Stat Sol (a) 1970;2:359–70.
[24] Klimanek P, Kuzel Jr. R. J Appl Cryst 1988;21:59–66.
[25] Ungár T, Tichy G. Phys Stat Sol (a) 1999;171:425–34.
[26] Ungar T, Gubicza J, Ribarik G, Zerda TW. In: Hjelm RP, Nakatani AI, Gerspacher M, Krishnamoorti R, editors, MRS Symposium filled and nanocomposite polymer materials, Boston: MRS, 2000, KK9.2.1-6.
[27] Ribárik G, Ungár T, Gubicza J. J Appl Cryst, in press.
[28] Tuinstra F, Koenig JL. J Chem Phys 1970;53:1126–30.
[29] Nakamura K, Kitajima M. Appl Phys Lett 1991;59:1550–2.